HHS Public Access

Author manuscript

Adv Healthc Mater. Author manuscript; available in PMC 2019 May 01.

Published in final edited form as:

Adv Healthc Mater. 2018 May ; 7(10): e1701415. doi:10.1002/adhm.201701415.

Novel 3D Hybrid Nanofiber Aerogels Coupled with BMP2 Peptides for Cranial Bone Regeneration

Dr. Lin Weng,
Department of Surgery-Transplant and Mary & Dick Holland Regenerative Medicine Program, College of Medicine, University of Nebraska Medical Center, Omaha, Nebraska 68198, United States

Dr. Sunil Kumar Boda,
Department of Surgery-Transplant and Mary & Dick Holland Regenerative Medicine Program, College of Medicine, University of Nebraska Medical Center, Omaha, Nebraska 68198, United States

Hongjun Wang,
Department of Surgery-Transplant and Mary & Dick Holland Regenerative Medicine Program, College of Medicine, University of Nebraska Medical Center, Omaha, Nebraska 68198, United States

Prof. Matthew J. Teusink,
Department of Orthopedic Surgery and Rehabilitation, University of Nebraska Medical Center, Omaha, Nebraska 68198, United States

Prof. Franklin D. Shuler, and
Department of Orthopaedic Surgery, Joan C. Edwards School of Medicine, Marshall University, Huntington, WV, 25755 United States

Prof. Jingwei Xie*
Department of Surgery-Transplant and Mary & Dick Holland Regenerative Medicine Program, College of Medicine, University of Nebraska Medical Center, Omaha, Nebraska 68198, United States

Abstract

An ideal synthetic bone graft is a combination of the porous and nanofibrous structure presented by natural bone tissue as well as osteoinductive biochemical factors such as bone morphogenetic protein 2 (BMP-2). In the present work, ultralight three-dimensional (3D) hybrid nanofiber aerogels composed of electrospun PLGA-collagen-gelatin (PCG) and Sr-Cu codoped bioactive glass (BG) fibers with incorporation of heptaglutamate E7 domain specific BMP-2 peptides have been developed and evaluated for their potential in cranial bone defect healing. The nanofiber aerogels were surgically implanted into 8 mm × 1 mm (diameter × thickness) critical sized defects created in rat calvariae. A sustained release of E7-BMP-2 peptide from the degradable hybrid

* jingwei.xie@unmc.edu.

Supporting Information

Supporting information is available from the author or Wiley Online Library.

aerogels significantly enhanced bone healing and defect closure over 8 weeks in comparison to unfilled defects. Histomorphometry and X-ray micro-computed tomography (μ-CT) analysis revealed greater bone volume and bone formation area in case of the E7-BMP-2 peptide loaded hybrid nanofiber aerogels. Further, histopathology data divulged a near complete nanofiber aerogel degradation along with enhanced vascularization of the regenerated tissue. Together, this study for the first time demonstrated the fabrication of 3D hybrid nanofiber aerogels from 2D electrospun fibers and their loading with therapeutic osteoinductive BMP-2 mimicking peptide for cranial bone tissue regeneration.

Graphical Abstract:

This study reports novel 3D hybrid nanofiber aerogels that topically deliver trace metal ions and BMP-2 peptides to promote neovascularization and cranial bone regeneration.

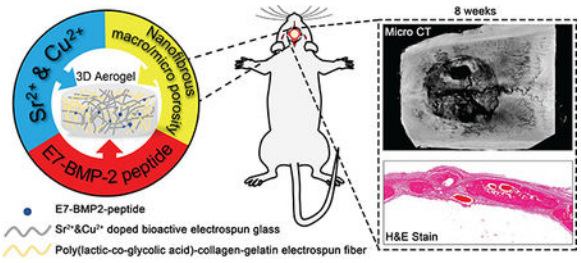

Keywords

Three dimensional; Hybrid nanofiber aerogel; Bioactive glass (BG) nanofibers; Bone morphogenetic protein (BMP-2) mimicking peptide; Cranial bone regeneration

1. Introduction

Critical sized bone defects during an osseous injury fail to heal during the life of the patient in the absence of secondary intervention.[1] The management of large bone defects remains a major clinical and socio-economical problem due to trauma, tumor removal or age related diseases such as osteoporosis.[2] In these cases, medical intervention will be required beyond stabilization, alignment and support of the damaged area in order to regrow bone and restore function. Currently, auto- and allografts are still the gold standard treatment for the treatment of critical sized bone defects despite of a number of drawbacks (e.g., limited resources, associated morbidity, mismatched size, immune rejection, and transmission of disease).[3] In United States alone, 1.3 million people undergo bone graft surgeries each year for skeletal defects resulting from either accidents or disease, which is the second most common tissue transplantation following blood.[4] Prosthetic implants (e.g., metals, ceramics, and plastic materials) which often result in stress shielding and reduction in bone density lack the ability to heal and grow, requiring surgery for repair of excessive wear and damage, and presenting complications when treating young patients where the body is growing over time.[5] There is an urgent need to develop an absorbable synthetic bone graft that can eliminate the need for a second surgical site to harvest autologous bone and issues associated with the use of allografts.

In the past few decades, great efforts have been devoted to either natural or synthetic materials as bone substitutes and considerable success has been achieved.[6] Several key factors have been considered as major contributors for bone regeneration. The grafting materials should be biocompatible and support cell attachment and growth, and if possible, degrade simultaneously during tissue regeneration. The porosity of the grafting materials should be sufficient to allow efficient cellular infiltration and proliferation within the structure. It should be supplemented with sufficient stimulants to boost angiogenesis and osteogenesis, and suppress osteoclast activity. For example, strategies often utilize soluble bone morphogenetic protein-2 (BMP-2) either physically adsorbed, covalently linked or encapsulated within 3D scaffolds/ microspheres to confer osteoinduction properties to the biomaterial/ implant.[7] However, depending on the method of immobilization, either the bioactivity is compromised or the growth factors eventually diffusing out of the scaffold necessitate a high dose, resulting in secondary effects on the surrounding host tissues and a reduced ability to locally influence the fate of cells inside a scaffold. The serious complications of high doses of BMP-2 protein include ectopic bone formation, osteoclast-mediated bone resorption, inappropriate adipogenesis, and unwanted immunogenic responses of the host.[8] On the contrary, the conjugation of BMP-2 proteins onto scaffolds for controlled release reduced their bioactivity and elicited lesser bone formation *in vivo*, compared to physically adsorbed BMP-2 protein.[9] Alternatively, short chain BMP-2 peptides have been developed to mimic the activity of BMP-2 proteins by binding to their cell receptors.[10] In contrast to soluble growth factors, calcium-coupling BMP-2 peptides (KIPKASSVPTELSAISTLYL) have been bound to scaffolds to facilitate bone regeneration.[11] Studies also showed that modified peptides derived from BMP-2 with a heptaglutamate domain (E7) significantly improved their binding to the hydroxyapatite surface through Ca coupling.[12] This method has several advantages including reducing the cost, enhancing the conjugation efficiency, and avoiding the short half-life and the side effects of released BMP-2 protein.

Studies have proposed the use of electrospun nanofibers as a grafting material for bone regeneration due to their biomimicry. However, traditional electrospinning typically produces uncontrolled and densely packed fibers, resulting in compact two-dimensional (2D) nanofiber mats/membranes which hinders cellular infiltration due to their low porosity.[13] Attempts also have been made to develop three-dimensional (3D) electrospun nanofiber scaffolds. Unfortunately, most approaches have been restricted to the fabrication of 3D nanofiber scaffolds composed of randomly oriented nanofibers and/or certain materials (e.g., with additives). These methods often led to insufficient thickness and/or restricted geometry and/or uncontrolled porosity and pore structures. Another class of bioactive bone substitute materials is comprised of mesoporous bioactive glass (BG) and BG nanofibers. The first BG, belonging to the 45SiO2–24.5Na2O–24.5CaO–6P2O5 (wt. %) system (45S5 Bioglass®), was developed by Hench *et al.* in the late 1960s and is in clinical use for orthopaedic and dental applications since 1985.[14] However, the BG materials produced previously are either in the bulk or granular form or fiber-type melt-derived glass with diameters of hundreds to tens of micrometers.[15] Such materials have lower osteoinduction properties due to their differences from the architecture of bone ECM. To mimic the 3D architecture and nanofibrillar structure of bone ECM, several studies attempted to fabricate BG nanofibers

using electrospinning.[16] However, due to the intrinsic limitations of traditional electrospinning technique, bioactive glass nanofibers generated previously were mainly in the form of 2D densely packed membranes. In addition, such 2D nanofiber membranes are very fragile due to the brittle nature of bioglasses, which makes them difficult to handle.

Our recent work developed a method to generate expanded 3D nanofiber scaffolds.[17] However, this method will not be suitable for expanding BG nanofibers due to their structural rigidity. Therefore, we have resorted to freeze casting of short nanofiber segments to form 3D hybrid nanofiber aerogels for the present study. In addition, strontium (Sr) aids in bone homeostasis by stimulation of osteoblast differentiation and bone formation,[18] as well as inhibition of osteoclastogenesis and bone resorption,[19] and copper (Cu) has been demonstrated to stimulate the proliferation of endothelial cells in a dose dependent manner *in vitro*, and promote wound healing by up-regulating VEGF expression.[20] Our recent study also demonstrated that binary doping of Sr and Cu enhanced osteogenesis and angiogenesis of progenitor cells cultured in BG nanofiber eluates while suppressing osteoclast activity *in vitro*.[21] Inspired by the formation of ultralight aerogels (porous solids) by the assembly of short electrospun fibers,[22] this study aims to develop and validate absorbable 3D hybrid nanofiber aerogels for cranial bone regeneration.

2. Results

2.1. Effect of freezing temperature on the morphology of 3D hybrid nanofiber aerogels

The 3D nanofibrous scaffold architecture with hierarchical pores was manipulated by a precise control over the freezing conditions of the segmented nanofiber suspension. Absolute ethanol cryopreserved at −80 ºC was used as the coolant for freezing the nanofiber suspensions in water. The coolant temperature and cooling rate of the electrospun nanofiber mixture suspensions were varied, in order to observe the effects of the freezing conditions on the aerogel macro and microstructure. To maximally reduce the temperature fluctuations of the coolant during the freezing process, a pre-cooled foam and copper ring mold glued to aluminum plates were used. The freezing was performed by rapid freezing of the nanofiber suspensions by cryopreserved ethanol of −30, −50 and −80 ºC for 1 min. During the initial 1 min cooling process, the rise in the coolant temperature was less than 5 ºC. The frozen nanofiber suspensions were subsequently transferred to −80 ºC for 10 min. Further, in order to ensure random pore distribution in the aerogel (Figure 1), metallic molds attached to an aluminum base were used to allow temperature gradients from both the axial and radial directions.

As shown in Figure 2, the final freezing temperature influenced the pore size distribution in the 3D nanofiber aerogel. As the rule of thumb, larger temperature gradient leads to smaller pores as the temperature gradient affects the periodic growth of ice crystals during freezing.[23] A similar phenomenon was observed in our case too. As evident from the SEM micrographs in Figure 2A to Figure 2C, the size of pores was around 30 μm and did not vary significantly for freezing temperatures of −30 to −80 ºC as the temperature difference was only −50 ºC. However, when liquid nitrogen was used as the coolant, a dramatic drop in the pore size was noted. The pores in Figure 2A-2C seemingly appeared as miniscule pores, though the overall porosity in Figure 2D was similar to the rest due to identical

concentration of the nanofiber suspensions. Apparently, such a small pore size imposed foreseeable difficulty for the LN_2 frozen aerogel as the implantation candidate for the intended bone tissue engineering application. Also among Figure 2A-2C, a slight difference in the thickness of the fiber wall of the aerogels may be noticed. For the sample frozen at −30 ºC, the wall was much thinner than the sample from −50 ºC or −80 ºC and its minor pores on the wall were larger, but sparser.

2.2. Effect of thermal treatment on the morphology of 3D hybrid nanofiber aerogels

After freeze drying of the 3D nanofiber aerogels, thermal treatment was performed to enhance the aerogel mechanical properties and to avoid disassembly of the nanofibers and micro-structure change. The thermal treatment temperature was chosen between 48 ºC - 52 ºC, which is in the range of the glass transition temperature (T_g) of PLGA (50:50). Absolute ethanol was used as the heat transfer medium during thermal crosslinking so as to prevent the dissolution of collagen and gelatin in water. Our results indicate that the nanofiber aerogel morphology was quite sensitive to the thermal treatment temperature and duration of thermal treatment. At 48 ºC, the efficiency of thermal treatment was low. Thermal treatment for 10 min at 48 ºC did not induce any change in the nanofiber aerogel morphology with the PLGA nanofibers remaining well separated from each other (Figure 3A). Upon increasing the thermal treatment duration to 120 min, numerous droplet-like features could be observed on the surface of the PLGA nanofibers and this can be attributed to melting and recrystallization of PLGA (Figure 3B). Such a thermal treatment condition was not favorable with regard to the aerogel stability as phase separation can dismantle the scaffold structure. When the temperature was increased to 52 ºC, thermal treatment greatly strengthened the 3D nanofiber aerogel. After 10 min, the PLGA nanofibers began to melt and fuse together (Figure 3C), thereby conferring strength and structural stability to the 3D nanofiber aerogel. An extended duration of thermal treatment to 120 min at 52 ºC promoted melting and PLGA recrystallization to a greater extent than that at 48 ºC (Figure 3D). Thus, thermal treatment at 52 ºC and 10 min was the optimal condition for enhancing aerogel stability without affecting the nanofiber morphology.

2.3. Effect of composition on the morphology and mechanical properties of 3D hybrid nanofiber aerogels

The ratio of PCG: BG fibers had a huge bearing on the morphology and stability of 3D hybrid nanofiber aerogels, especially after thermal crosslinking. Our goal was to incorporate larger amounts of the doped BG fiber in the 3D hybrid nanofiber aerogels so as to realize therapeutic release of Sr^{2+} and Cu^{2+} ions to promote neobone formation and vascularization, respectively. Towards that end, 3D hybrid nanofiber aerogels with different ratios of PCG and BG fibers were fabricated by freeze casting, followed by thermal crosslinking. Particularly, the stability, morphology and mechanical properties by compression were investigated. Physically, the color of the gross 3D PCG nanofiber aerogels were pale yellow (Figure 4A) and the color turned white to greyish (Figure 4E) with increase in the content of BG fibers. Also, a distinct difference in the morphology of the 3D hybrid nanofiber aerogels was observed under SEM, especially that of the fiber wall. For the pristine PCG 3D nanofiber aerogel, the fiber walls were thinner and the fibers were interwoven to form a thin plain (Figure 4A). With the gradual replacement of the long PCG fibers with short BG

fibers, the fiber walls appeared thicker probably due to the opposition of the BG fiber against compression by the growing ice crystals during freezing. When the BG fiber content reached 75 wt% (PCG:BG = 25:75), the 3D aerogel walls became increasingly branched, extending randomly to the adjacent space (Figure 4E). It was extremely difficult to increase the glass fiber composition beyond 75 wt% due to two major limitations. Firstly, the solution mixture of the BG and the PCG fiber started to aggregate and sediment severely, even though both the polymer and glass fibers exhibited negative surface charge/ Zeta potential (data not shown) that could stabilize the nanofiber suspensions. Secondly, the fabricated scaffolds collapsed or were impossible to handle for > 75 wt% of BG fiber in the 3D hybrid nanofiber aerogel.

Further, the compression moduli of the 3D hybrid nanofiber aerogels are commensurate with the scaffold stability. It was expected that the addition of BG fibers would increase the compressive strength of the aerogel as bulk bioactive glasses possess compressive moduli of the order of 10 to 100 MPa.[24, 25] [25] However, the compression strength of the hybrid aerogels decreased as more BG was incorporated. Figure S2 and S3 are representative stress-strain curves recorded during uniaxial compression tests of the 3D nanofiber aerogels. Figure 4F indicates that the PCG 3D nanofiber aerogel has the highest compressive modulus, while incorporation of BG led to an exponential drop in the aerogel stiffness. When the BG content was increased to 75 wt%, the compressive modulus of PCG: BG (25:75) was merely one fifth of the PCG:BG (100:0) 3D nanofiber aerogel. This contrasting phenomenon can be rationalized in that the actual compression test was performed on the aerogel with a small ε (25%), in which the cross-linked network was compressed, instead of the individual nanofibers. A close observation of Figure 4 will reveal that only the PCG nanofiber actively took part in the heat-induced crosslink, while the BG nanofibers were loosely attached to the PCG nanofiber network. Thus, the compression strength of the aerogel mainly depends on the amount of thermally cross-linked PCG nanofibers. Also, the compression strength does not vary linearly with the content of PCG nanofibers. This can be explained through a simplified model in which each piece of nanofiber is treated equally. We also assume that only neighboring PCG nanofibers can crosslink. Thus, the chance to have a two piece cross-linked network is the square of the ratio of PCG nanofiber, and if we require a network to have more pieces of PCG nanofibers, the chance becomes a power function, one of whose form was adopted to plot the function to fit the relation between the PCG nanofiber content and compression strength.

2.4. Bioactivity of the 3D hybrid nanofiber aerogels in SBF

The 3D polymer and hybrid nanofiber aerogels were immersed in SBF to evaluate their bioactivity *in vitro*. The kinetics of calcium apatite formation on the 3D nanofiber aerogels are indicative of their bioactivity. After two weeks of incubation in SBF, we were able to observe apatite-like structures on all the compositions of the 3D hybrid nanofiber aerogels (PCG: BG = 100:0, 75:25, 60:40 and 50:50) (Figure 5A-5D), and to a small extent in PCG: BG = 25:75. This is commensurate with our earlier findings, wherein Sr and Cu co-doped BG nanofibers retarded apatite mineralization in SBF in comparison to the undoped or Ca-doped BG nanofibers.[21] The released Sr interferes with the mineralization of hydroxyapatite by competitively binding to phosphate as opposed to Ca. Also, the released

Cu tends to precipitate in alkaline pH by interacting with bicarbonate and hydroxyl ions in the SBF. Therefore, it was not surprising that the 3D hybrid nanofiber aerogels exhibited decreased levels of calcium apatite formation with increasing content of the Sr-Cu co-doped BG nanofibers. The following is the decreasing order of bioactivity exhibited by the composite 3D nanofiber aerogels – PCG: BG (100:0 > 75:25 > 60:40 > 50:50 >> 25:75). Furthermore, the PCG 3D nanofiber aerogel was uniformly covered with dense apatite (Figure 5A), while in the case of PCG-BG (25:75) 3D hybrid nanofiber aerogel, the calcium phosphate deposition was sparse and only occurred at few sites (Figure 5E). Thus, the SEM images together undoubtedly demonstrate that the addition of PCG nanofibers to bioactive glass fibers enhanced the bioactivity of the 3D hybrid nanofiber aerogels, while also enhancing the mechanical properties of the aerogel as described in the previous section.

2.5. Loading and release of E7-BMP-2 peptide from 3D hybrid nanofiber aerogels

A previous study demonstrated comparable osteoinductive efficacy of heptaglutamate E7 domain modified BMP-2 peptide and recombinant human BMP-2 protein loaded on anorganic bovine bone graft for ectopic bone formation in rats.[26] Taking cue from that study, the PCG- BG (60:40) 3D hybrid nanofiber aerogels were loaded with E7-BMP-2-FITC peptide, presuming the coupling of the peptide to the Ca present in the BG fibers. The FITC tagged E7-BMP-2 peptide was used to determine the loading and release profiles of the peptide from the 3D hybrid nanofiber aerogels. Figure 6A shows the loading and release kinetics of E7-BMP-2-FITC peptide from the hybrid nanofiber aerogels. The data shown in Figure 6A indicates that ~10 μg of the peptide was incorporated to the PCG-BG (60:40) 3D nanofiber aerogels and 90% of the peptide was released within the first week followed by sustained release up to 4 weeks. The rapid release profile of the peptide may be attributed to ineffective Ca coupling of the peptide due to the small percentage of calcium in the BG fiber component of the hybrid aerogels. Figure 6B, 6C and 6D are fluorescence microscopy images of the 3D PCG:BG = 60:40 hybrid nanofiber aerogels after E7-BMP-2-FITC peptide loading for 24 h, peptide release for 3 weeks and 4 weeks, respectively. It is probable that the remnant peptide present after 4 weeks may be released upon scaffold degradation *in vivo*.

2.6. Cranial bone regeneration in vivo

The premise for the current study was to demonstrate the osteoinductive efficacy of strontium and copper co-doped bioactive glass fibers for cranial bone regeneration. Towards this end, our objective was to incorporate as much amount of bioactive glass fibers as possible into the 3D hybrid nanofiber aerogel without compromising on their mechanical stability. Among the fabricated scaffolds, the PLGA:BG (60:40) hybrid aerogel composition satisfied both the requirements. Summarizing, based on the mechanical property and composition, we chose PLGA:BG (60:40) as the test groups for *in vivo* studies, both without and with loading of E7-BMP-2 peptide.

2.6.1. Micro-CT analysis—Micro-computed tomography was used to quantitatively assess the rat calvarial bone defect healing induced by the 3D hybrid nanofiber aerogels after 4 and 8 weeks of implantation. Representative micro-CT images for the various implant groups are shown in Figure 7A1-C2. Also, the new bone formation at the periphery of the

circular cranial defects has been demarcated from the old bone by a red circle to indicate the region of interest used for analysis. The micro-CT analysis indicates an obvious increase in x-ray radiopacity due to new bone formation between 4 weeks and 8 weeks for all the implant groups. Among the different groups, the determined bone formation area and bone volume were maximum for the E7-BMP-2 peptide loaded 3D hybrid aerogel (PCG:BG = 60:40). Also, the neobone for E7-BMP-2 peptide loaded hybrid aerogel group exhibited extremely high radiopacity, with high-density bone mineral covering more than half of the cranial defect over 8 weeks. The statistics of the micro-CT analysis presented in Figure 7D and 7E suggest 65% closure of the bone defect volume and 68% coverage of the defect area. On the contrary, the 3D hybrid nanofiber aerogel devoid of the osteoinductive peptide did not elicit significant new bone formation in comparison to the unfilled defect, both after 4 and 8 weeks. Nevertheless, the 3D hybrid nanofiber aerogels incorporated with low amount of E7-BMP-2 peptide elicited remarkable new bone formation in Ø8 mm × 1mm (thickness) critical sized cranial bone defects in rat calvariae.

2.6.2. Histomorphometric analysis—Finally, the new bone tissue and neovasculature formed in all the implant groups were quantitatively studied by histomorphometric analysis following H&E and Masson's trichrome staining. Most importantly, the 3D nanofiber aerogel implants did not trigger any inflammatory and/ or foreign body reaction as evident from the absence of foreign body giant cells. Both H&E as well as Masson's trichrome staining reveal a highly retarded new bone formation in the control unfilled cranial defects. The only new bone in the control group was along the periphery of the defect with limited size and it did not develop significantly from 4 to 8 weeks (Figure 8A, D; Figure 9 A,D). Also, a large percentage of the regenerated tissue was composed of loose fibrous connective tissue instead of dense bone tissue in the unfilled defects. On the contrary, the 3D hybrid nanofiber aerogel based implant groups exhibited signs of developing bone trabeculae along with blood capillaries in the porous scaffolds at 4 weeks (Figure 8B-C; Figure 9B-C). Particularly, the density of blood vessels was maximum for the 3D hybrid nanofiber aerogels (PCG:BG = 60:40), both with and without E7-BMP-2 peptide loading after 4 weeks (Figure 8B-C; Figure 9B-C) and 8 weeks (Figure 8E-F; Figure 9F-F) of implantation. At 8 weeks, the thickness of the new trabecular bone was significantly higher in the E7-BMP-2 peptide incorporated 3D hybrid nanofiber aerogel group compared to all the other groups. Further, the new bone formation occurred at the periphery as well as the middle of the defect leading to a near complete closure of the calvarial defect. In case of the 3D hybrid nanofiber aerogels devoid of the peptide, the new bone formation was restricted to the defect periphery or the middle region without completely bridging the defect cavity. A histomorphometric analysis of the vascularization of the regenerated bone tissue was performed from multiple slides/ tissue sections ($n \geq 12$) prepared from the rat calvariae retrieved from the different implantation groups at 4 and 8 weeks. Additional histological images used for bone morphometric analysis are shown in Figure S4A-F and Figure S5A-F. Figure 10 presents the density of neovasculature (vessels/ mm^2) formed in the regenerated tissue at 4 and 8 weeks. The density of blood vessels in the regenerated tissue was higher in both the 3D hybrid aerogel groups (with and without E7-BMP-2 peptide) in comparison to the unfilled defect. Also, the 3D nanofiber aerogels were largely degradable with few scaffold remnants seen in all the implant groups even after 8 weeks.

3. Discussion

Traditionally, polymeric nanofiber scaffolds for tissue engineering are fabricated by electrospinning, phase separation and self-assembly of specific types of polymers.[27] Among them, electrospinning is a highly versatile technique to generate scaffolds with nanofiber topography, mimicking the extracellular matrix (ECM) of native tissue. However, the pore size of electrospun nanofiber mats is too small hindering adequate cell infiltration although microfibers have larger pores depending on the fiber diameter.[28] This has necessitated the development of 3D scaffold fabrication methods from 2D nanofiber mats. Among them, expansion of polymeric nanofiber mats into 3D structures by gas foaming was developed previously from our group.[17] Also, 3D scaffolds of polymers can be formed from fragmented electrospun nanofibers by freeze casting and freeze drying of the aqueous fiber suspensions, followed by thermal crosslinking. In a previous study, PCL-PLA nanofiber blends were fragmented by cryo-milling and thermally induced nanofiber self-agglomeration (TISA) technique was applied for the fabrication of 3D nanofibrous scaffolds for craniofacial bone regeneration.[29] In another study, electrospun gelatin/PLA fibers were homogenized and the nanofiber suspension was freeze cast, dried, thermally and chemically crosslinked (EDC/NHS) to obtain 3D nanofibrous scaffolds for cartilage tissue engineering.[30] The aforementioned studies focus on pristine polymer/ co-polymer nanofiber aerogels, while literature reports of inorganic aerogels are also well known.[31] To the best of our knowledge, for the first time we report the fabrication of 3D hybrid nanofiber aerogels composed of organic polymer PCG and inorganic BG fibers. In the study, the freeze casting of homogenized PCG and BG nanofiber suspensions and thermal crosslinking conditions were optimized to obtain stable 3D hybrid nanofiber aerogels. Various compositions of PCG:BG hybrid nanofiber aerogels were prepared and we observed that BG content ≥ 75 wt % collapsed the 3D scaffold structure. This could arise from the lack of structural support from the polymer crosslinks for BG content ≥ 75 wt% (PCG: BG = 25:75). For lower BG content ≤ 40 wt% (PCG: BG = 60:40), the negative surface charges of both the BG fibers and PCG fibers stabilize the nanofiber suspension without precipitation of the heavier BG fibers during freeze casting of the homogenized mixture. After freeze drying, the hybrid aerogels were further strengthened by effective thermal crosslinking. In a previous work, hybrid composites of BG nanofibers dispersed in collagen matrix at 40 wt% was structurally optimal for biomineralization in SBF and induced higher alkaline phosphatase (ALP) activity in osteoprogenitor cells, *in vitro*.[32] Taking cue from the previous study as well as our own observations on scaffold stability, the PCG: BG = 60:40 compositions of the 3D hybrid nanofiber aerogels were chosen for the animal experiments.

Although BG fibers have been predicted as the next generation orthopaedic/dental biomaterials,[33] they are mechanically brittle such that it is not possible to perform tensile or flexural tests on glass nanofibers. However, similar tests may be performed on microfibers and the tensile strength was reported to vary inversely with fiber diameter.[34] In order to overcome the poor mechanical properties of BG nanofibers, 3D hybrid nanofiber aerogels have been fabricated together with polymer nanofibers. The differences in the mechanical properties of the 3D nanofiber aerogels arise from the proportion of thermally cross-linked PCG nanofibers in the hybrid aerogels. The compressive moduli were observed to increase

with polymer content as greater polymer crosslinking enhanced the aerogel mechanical properties. The 3D hybrid nanofiber aerogels have been successfully used for cranial bone defect healing in the current study. As the cranium is a non-load bearing bone, the 3D hybrid nanofiber aerogel may be a good fit for cranial bone tissue engineering. Further, it is also possible to produce complex shapes with the 3D nanofiber aerogels capable of fitting bone defects using a mold generated by 3D printing technique based on the 3D imaging of bone defects.[35] However, the 3D hybrid aerogels may need further toughening in order to applied for tissue engineering of load bearing long bones.

Although the premise for performing the current study was the osteoinductive effect of the Sr-Cu co-doped BG nanofibers as reported in our recent *in vitro* study,[21] the *in vivo* results suggest otherwise. The bone forming ability of the 3D PCG: BG = 60:40 hybrid nanofiber aerogel is comparable to that of the unfilled defect. This implies that the 3D hybrid nanofiber aerogel by itself is not effective in eliciting healing of critical sized cranial defects. Perhaps, the concentration of the released Sr^{2+} and Cu^{2+} from the hybrid aerogels is below the therapeutic levels necessary for bridging such large bone defects. Another explanation could be the mismatch between the compression strength of the 3D nanofiber aerogels (0.5 to 2.5 MPa) and that of the native cranial bone (8000 MPa),[36] as mechanotransduction can play an important role in the healing of mechanosensitive bone tissue.[37] However, the 3D hybrid aerogels do promote the sprouting of new blood vessels in the regenerated fibrous connective and bone tissue in comparison to the defect only group (Figure 10). Overall, the E7-BMP-2 peptide loaded 3D hybrid nanofiber aerogel is the most potent through the regeneration of vascularized bone tissue as indicated by micro-CT and histomorphometric analysis. Additionally, the Sr-Cu co-doped BG fibers can confer antibacterial properties to the 3D hybrid nanofiber aerogel. This is important in the light of the large percentage (≥ 60%) of graft failure in cranioplasty due to surgical site infection.[38]

Of late, bone morphogenetic protein mimicking peptides designed from the amino acid sequence of the active sites of BMP-2 protein are being shown to overcome the drawbacks of whole BMP-2 protein, while retaining the osteoinductive properties.[39, 40] Such peptides presented on 3D alginate hydrogels scaffolds by chemical conjugation induced osteogenic differentiation of osteoprogenitor cells *in vitro*.[11] Particularly, the engineering of peptide with the heptaglutamate E7 domain to confer enhanced calcium binding properties as necessary to deposit bone mineral led us to choose this peptide for our study. Moreover, recent literature suggests comparable osteoinductive efficacy of E7-modified BMP-2 mimicking peptide to full length recombinant BMP-2 (rBMP-2) protein, wherein the peptide promoted greater bone formation in ectopic and mandibular defects without triggering any inflammation.[26] Two more peptides designated as P24 and P28 with amino acid residues 73–92 of the knuckle epitope of BMP-2 protein and additional aspartic acid residues, 3 and 7 for P24 and P28, respectively were designed. Both P24 and P28 BMP-2 mimicking peptides exhibited comparable bone formation to BMP-2 protein loaded scaffolds *in vivo.*[40, 41] However, in both the previous studies, large amounts of peptide of the order of 1–3 mg was loaded per scaffold to elicit bone healing, where as in our case, only ~10 μg of E7-BMP-2 peptide per scaffold was sufficient to evoke more than 60% defect closure over 8 weeks. Thus, it may be concluded that the 3D hybrid nanofiber aerogels are excellent synthetic matrices for efficient loading and delivery of osteoinductive peptides/ions

necessary for cranial bone defect healing. However, a fast release of the peptide was recorded due to its desorption from the 3D hybrid nanofiber aerogel. A controlled release of the osteoinductive peptide could be achieved in the following two ways - (i) Mineralization of the 3D nanofiber aerogel with CaP or incorporation of CaP in the scaffold composition can enhance the binding of the E7-BMP-2 peptide and also promote a slow controlled release of the peptide, (ii) Immobilization of the peptide onto the nanofiber aerogel through EDC/NHS chemistry or linker molecules such as biotin and streptavidin. These approaches for the sustained release of E7-BMP-2 and/or other osteoinductive peptides will be experimented in our future studies. Further, taking cue from a recent review, we plan to design collagen binding osteoinductive peptides for wound healing and bone tissue regeneration.[42] Taken together, the 3D hybrid nanofiber aerogels incorporated with osteoinductive peptides is a promising direction for the development of synthetic bone grafts. Another approach for promoting bone tissue ingrowth into the defect area is through the fabrication of porous scaffolds with radially aligned pores by directional freezing. This method was adopted for the fabrication of oriented cellular foams from cellulose nanofibril dispersions.[43] A similar strategy can be used with homogenized nanofibers to fabricate radially aligned nanofiber aerogels.

Overall, it is worthwhile mentioning that the Sr^{2+} and Cu^{2+} dopant ions release from the BG fibers and the E7-BMP-2 peptide can work synergistically to promote new bone formation and vascularization of the calvarial defect, though not effectively by the 3D hybrid nanofiber aerogel itself. As in a previous study where rhBMP-2 protein and alendronate were loaded into a collagen sponge,[44] we intend to incorporate our 3D hybrid nanofiber aerogels with combinations of osteogenic, anti-osteoclastogenic, antibacterial and angiogenic factors to achieve complete regeneration of healthy vascularized bone tissue in our future studies.

4. Conclusion

We demonstrated for the first time the fabrication of 3D hybrid nanofiber aerogels composed of segmented electrospun polymer and BG nanofibers. We optimized the morphology, mechanical property, and composition of aerogels by varying the freezing temperature, ratio between polymer and glass nanofibers, cross-linking temperature and duration. The optimized nanofiber aerogels containing collagen and bioactive glasses had hierarchical cellular-structure, and interconnected pores and nanofibrous architecture, recapitulating the native architecture and composition of bone ECM. We further demonstrated that E7-BMP-2 peptides incorporated 3D hybrid nanofiber aerogels can induce ~60–70% closure of critical-sized (8 mm) rat calvarial bone defects. Further, the high surface area to volume ratio of such nanofiber aerogels can be exploited for optimal loading of osteoinductive and/or angiogenic factors for accelerated regeneration of neovascularized bone. Taken together, the 3D hybrid nanofiber aerogels showed a great promise for cranial bone regeneration.

5. Experimental Section

5.1. Fabrication of PCG nanofibers and Sr and Cu co-doped BG nanofibers

The electrospinning set-up used in the present work is similar to that described in our previous publication, where the mandrel collector was stationed above the syringe needle

and pump to recruit gravity to affect the fiber collection.[21] The recipe for the electrospinning of Sr and Cu co-doped BG nanofibers is a slight modification of an existing recipe,[45] from one of earlier published works. It consists of two portions namely the sol-gel mixture and polymer additive to adjust the solution viscosity for electrospinning. The first portion is comprised of 1.34 g of tetraethyl orthosilicate (Sigma-Aldrich), 0.116 g of triethyl phosphate (Aldrich), 0.148 g of $Ca(NO_3)_2{\cdot}4H_2O$ (Sigma-Aldrich), 0.132 g of $Sr(NO_3)_2$ (Sigma-Aldrich), 0.200 ml 0.0053g ml^{-1} $CuCl_2$ (Sigma-Aldrich) aqueous solution, 0.100 ml of HCl (Sigma-Aldrich) solution (1 mol l^{-1}), 4.00 ml of ethanol (DECON), and 3.00 ml of D.I water. The second polymeric portion of polyvinylpyrrolidone (PVP) (Sigma-Aldrich, Mw 1,300,000) was prepared by dissolving 1.65 g of PVP in 10.0 mL of absolute ethanol. Prior to electrospinning, a 1:1 mixture of two portions was stirred for 2 hours at 4 ˚C. The electrospinning was performed using appropriate DC voltage (~15 kV) and needle tip to collector distance (10 – 15 cm) apart from a typical solution feeding rate of 0.60 ml h^{-1}. The composite nanofibers were collected by a slowly rotating mandrel, pre-coated with a memory layer of poly (ε-caprolactone) (PCL) (Sigma-Aldrich, Mw 80,000) fibers. Both the polymer components, PCL and PVP in electrospun fibers were later removed by sintering the collected composite fiber mats in a muffle furnace at 600 ˚C for 5 h in air.

To prepare PLGA-collagen-gelatin (PCG) electrospun nanofibers, we used a similar electrospinning setup as the BG electrospun fibers. The solution for the PCG electrospun nanofibers was made by dissolving 0.750 g 50:50 PLGA (LACTEL absorbable polymers 50:50, Mw 30,000 – 60,000), 0.375 g collagen type I (Calf skin lyophilized, Elastin Products Co., Inc, Owensville, USA), and 0.375 g gelatin (from porcine skin powder, Type A, Sigma-Aldrich) in 20.0 ml of hexafluoroisopropanol (Acros). After stirring for 1 h, the solution was stored at 4 ˚C. For electrospinning PCG fibers, the typical feeding rate of the solution mixture was 0.40 ml h^{-1}, while the applied DC voltage and distance between the spinneret and the collecting mandrel were 15 kV and 15 cm, respectively. The rotation speed of the collecting mandrel was fast enough to guarantee the aligned feature of the collected electrospun nanofiber. The as spun PCG fibers were cross-linked by glutaraldehyde (GA) vapors from a 25% ethanolic solution of GA for 24 h.

5.2. Freeze casting and thermal treatment of the hybrid 3D nanofiber aerogel

The minced BG electrospun fiber and the scissored pieces of PCG electrospun fiber were weighted into separate glass vials. Deionized water was added to the glass vials to wet the electrospun fiber and the fiber concentration was set to 40 mg mL^{-1}. The wetted fibers were homogenized by a 20 kHz probe sonicator (Qsonica 500) equipped with a 1/8-inch probe under ice-cold conditions for 10 min using on/off cycles of 10/20 s and 20% amplitude. After the electrospun fibers were fragmented into homogenous broken segments, the polymer and glass fiber suspensions were mixed in certain ratios of scaffold recipes and the mixtures were homogenized once again. The homogenous mixture was pipetted into copper rings molds glued to an aluminum plate. The mixtures were rapidly frozen done by cryopreserved ethanol in −80 ºC deep freezer. The frozen rings were immediately transferred to a −80 ˚C refrigerator for 10 min and freeze dried at −55 ºC in a lyophilizer (Labconco, Kansas, USA) for 72 h.

The freeze-dried samples were thermally treated in absolute ethanol pre-warmed to the required temperature in a water bath for 10 min. The thermal treatment is essentially a physical fusion of the nanofibers at the points of overlap in the aerogel without the formation of specific chemical bonds as in chemical cross-linking. The purpose of thermal treatment was to enhance the mechanical property of nanofiber aerogels through the fusion of polymer fibers and bioactive glass nanofibers. Upon thermal treatment, solvent exchange with cold deionized water was performed three times at intervals of 2 h. Vacuum was applied to remove the air bubbles trapped in the 3D nanofiber aerogel and gentle tapping was used to remove the aerogels from the copper ring molds. Subsequently, the aerogels were shaped into samples of 8 mm diameter and 1 mm thickness by sectioning with a cryotome and freeze dried for 24 h.

5.3. Characterization of PCG, Sr and Cu co-doped BG electrospun fibers and 3D nanofiber aerogels

The surface morphology of the fabricated 3D nanofiber aerogels and their precursor PCG and Sr-Cu codoped BG electrospun fibers was characterized by scanning electron microscopy (FE-SEM; Hitachi S4700). To avoid charging, the composite samples were fixed on a metallic pin stubs with double-sided conductive carbon tape and coated with chromium for 240 seconds using a sputter coater. The SEM images were acquired at an accelerating voltage of 5 kV.

5.4. Mechanical testing

The mechanical properties of the different compositions of the 3D nanofiber aerogels were recorded with an Instron 5640 universal test machine (UTM). The compression tests were carried out on cylindrical samples of 8 mm diameter and 5–10 mm height. The samples were loaded using a crosshead speed of 0.005 mm s^{-1} to 70% of their original height. The elastic modulus values were determined from the linear fits of the acquired stress-stain curves.

5.5. Assessment of bioactivity of the 3D nanofiber aerogel in simulated body fluid

The bioactivity of the consolidated 3D nanofiber aerogels was determined by immersion in simulated body fluid (SBF) using the SBF recipe developed by Kokubo, et al.[46] The biomineralization was performed by incubating the 3D aerogels in SBF at 37 °C for 2 weeks. Fresh SBF solution was replenished each week. Post mineralization, the aerogels were washed thrice using deionized water at 10 min intervals and freeze dried before examination under SEM.

5.6. Loading and release of E7-BMP-2 peptide from the 3D nanofiber aerogel

The 3D polymer-glass hybrid nanofiber aerogels were loaded with E7-BMP-2 peptide. The synthesized modifications of the peptide sequence were prepared by Genscript Co., Inc, including E7-BMP-2 peptide (EEEEEEEKIPKASSVPTELSAISTLYL, 3022.28 g mol^{-1}), and E7-BMP-2-fluorescein isothiocyanate (FITC) (EEEEEEEKIPKASSVPTELSAISTLYL-FITC, 3524.82 g mol^{-1}). The two peptides were reconstituted in tris-buffered saline (TBS, pH = 7.4) at 1.0 mg ml^{-1}, and the aliquots were stored at −24 °C. The FITC-tagged peptide was used for studies of peptide retention and release, whereas untagged peptide was used for

the bone regeneration studies *in vivo*. The aerogels were immersed in 35 μg ml^{-1} of the peptide in TBS for 24 h at room temperature. As performed in a previous study, the difference in the concentration of the peptide solution before and after immersion of the 3D nanofiber aerogels was used to estimate the amount of peptide loaded.[47] The peptide release from the aerogels was periodically recorded by measuring the fluorescence intensities of E7-BMP-2-FITC using excitation and emission wavelengths of 485 and 528 nm, respectively.

5.7. Bone regeneration in vivo

The *in vitro* osteogenesis of BMP-2 mimicking peptides conjugated to alginate hydrogel was demonstrated in murine derived mesenchymal stem cells by Madl *et al*. [11] Further, the E7-BMP2 peptides have been demonstrated in the literature for their efficacy in enhancing bone regeneration *in vivo*. [12, 26] These reports undoubtedly establish the osteoinduction property of these peptides and led us to directly test our nanofiber aerogels loaded with the E7-BMP-2 peptide *in vivo*.

5.7.1. Critical-sized cranial bone defect model—Care and use of laboratory animals was followed in accordance with the animal experimentation protocol approved by the Institutional Animal Care and Use committee (IACUC) of the University of Nebraska Medical Center. All the surgical, post-surgical and tissue processing procedures are in agreement with the standard procedures for evaluating bone regeneration in critical-sized calvarial defects in rats.[48] Twelve week-old Sprague Dawley rats (male) were used as the animal model to create critical-sized cranial defects for *in vivo* study. Prior to the surgery, the rats were acclimatized to the animal housing facility cages, fed on standard laboratory diet and maintained at ambient temperature. For the surgery, the rat scalps were shaved and cleaned and with antiseptic (povidone-iodine) and ethanol swabs. Then, an incision upto the cranial periosteum was created (Figure S1A). After exposing the calvaria, a circular defect of 8 mm diameter was made within the parietal bone by using a trephine bur mounting on a dentist drill. The heat generated from the drilling was dissipated by irrigating the defect site with sterile saline intermittently. While making the defect, it was ensured that both, the periosteum and underlying dura mater were kept intact. After removing the cut out calvarial disk, sterile hybrid nanofiber aerogels of Ø8 mm × 1 mm (thickness) completely soaked in sterile saline were placed into the cranial defects (Figure S1B). The overlying tissue was sutured with #6/0 line (Figure S1C), which were removed 6 days after surgery. A total of 36 rats divided into 3 groups (n=12) were used for the animal experiments. They were as follows: (1) The negative control group without scaffold implantation, (2) 3D PCG-BG (60:40) hybrid aerogel implantation group, and (3) E7-BMP2 peptide loaded 3D PCG-BG (60:40) nanofiber hybrid aerogel implantation group. The rats were sacrificed at 4 and 8 weeks. Following euthanization by CO_2 asphyxiation, the rat calvariae were retrieved, fixed in 10% formalin for 3 days and then transferred to 70% ethanol for further radiographic and histological analysis.

5.7.2. Radiographic analysis—The formalin fixed samples were first scanned with a high-resolution micro-CT scanner (Skyscan 1172, Kontick, Belgium) using x-ray tube voltage of 70 kV, current of 114 μA and slice thickness/ slice increment of 8.71 μm. The

radiographic analysis was done by CT analyzer software® (Bruker microCT). A 3D reconstruction of the skull bone was performed from multiple scan slices. In the region of interest, the bone volume was determined by applying appropriate threshold to distinguish the old and new bone. For calculating the bone volume percentage, the bone volume obtained from micro-CT analysis was divided by the defect volume. The defect volume was calculated as $\pi r^2 t$, where diameter = 2r = 8 mm and thickness = t = 0.6 mm. The thickness of the rat skull has been reported to vary from 0.5 – 0.7 mm, depending on the body mass. [49, 50] Additionally, the ImageJ software (NIH, Bethesda, MD, USA) was used to analyze the 3D model to obtain the bone formation area percentage.

5.7.3. Histolopathological analysis—Following the radiographic analysis, the retrieved rat calvariae were decalcified in Rapid Cal Immuno™ (BBC Biochemical, Mount Vernon, WA) for 2 weeks with solution refreshment every two days. After decalcification, the specimens were bisected, dehydrated in an increasing gradient series of ethanol (70–100%), and embedded in individual paraffin wax blocks. From the paraffin embedded tissue, 4 μm thick sections were prepared with the help of a microtome. Multiple sections were prepared per sample and stained with either Hematoxyline and Eosin (H&E) or Masson's trichrome, following the manufacturer's protocols. The stained sections were examined using a Ventana's Coreo Au slide scanner. 3.1.3. For bone histomorphometric analysis, a minimum of 12 slides/ tissue sections were used to quantify the density of new blood vessels or neovasculature. The quantification of the neovasculature was performed as reported in one of our previous publication by Jiang *et al.* [51] Briefly, the histology slide images were analyzed for the density of blood vessels using Ventana image viewer v. 3.1.3. For each slide, two snapshots were taken at different locations on the tissue section at 4x, 10x and 40x. The number of blood vessels were counted and normalized to the tissue area using the software.

5.8. Statistical analysis and image editing

For all the data presented in the current study, the statistical analysis was carried out using IBM SPSS Statistics software 20. All data are presented as means ± standard deviation (SD) of n=12 replicates per group. The statistical significance was determined by performing one-way analysis of variance (one way ANOVA) with Tukey test and with a statistical significance accepted at $p < 0.05$ and 0.005, where p denotes the probability that there is no significant difference between the means of the groups compared. For the histology images, the brightness and contrast were adjusted uniformly for all the images in the same figure for better visibility.

Supplementary Material

Refer to Web version on PubMed Central for supplementary material.

Acknowledgements

This work was supported by the grant from the National Institute of General Medical Science (NIGMS) at National Institute of Health (NIH) (2P20 GM103480–06), Nebraska Regenerative Medicine Program Pilot Project Grant, and startup funds from the University of Nebraska Medical Center.

References

[1]. Sanders DW, Bhandari M, Guyatt G, Heels-Ansdell D, Schemitsch EH, Swiontkowski M, Tornetta P, 3rd, Walter S, J. Orthop. Trauma 2014, 28, 632. [PubMed: 25233157]

[2]. Sterling JA, Guelcher SA, Curr. Osteoporos. Rep 2014, 12, 48. [PubMed: 24458428]

[3]. Van Heest A, Swiontkowski M, Lancet 1999, 353, S28.

[4]. Boyce T, Edwards J, Scarborough N, Orthop. Clin. North Am 1999, 30, 571. [PubMed: 10471762]

[5]. Cheal EJ, Spector M, Hayes WC, J. Orthop. Res 1992, 10, 405. [PubMed: 1569504]

[6]. Roberts TT, Rosenbaum AJ, Organogenesis 2012, 8, 114. [PubMed: 23247591]

[7]. Suliman S, Xing Z, Wu X, Xue Y, Pedersen TO, Sun Y, Døskeland AP, Nickel J, Waag T, Lygre H, Finne-Wistrand A, Steinmüller-Nethl D, Krueger A, Mustafa K, J. Control. Release 2015, 197, 148. [PubMed: 25445698]

[8]. James AW, LaChaud G, Shen J, Asatrian G, Nguyen V, Zhang X, Ting K, Soo C, Tissue Eng. Part B Rev 2016, 22, 284. [PubMed: 26857241]

[9]. Patel JJ, Flanagan CL, Hollister SJ, Tissue Eng. Part C Methods 2015, 21, 489. [PubMed: 25345571]

[10]. Kanie K, Kurimoto R, Tian J, Ebisawa K, Narita Y, Honda H, Kato R, Materials (Basel) 2016, 9.

[11]. Madl CM, Mehta M, Duda GN, Heilshorn SC, Mooney DJ, Biomacromolecules 2014, 15, 445. [PubMed: 24400664]

[12]. Culpepper BK, Phipps MC, Bonvallet PP, Bellis SL, Biomaterials 2010, 31, 9586. [PubMed: 21035181]

[13]. Ma B, Xie J, Jiang J, Shuler FD, Bartlett DE, Nanomedicine (Lond) 2013, 8, 1459. [PubMed: 23987110]

[14]. Greenspan DC, Int. J. Appl. Glass Sci 2016, 7, 134.

[15]. Jones JR, Acta Biomater. 2013, 9, 4457. [PubMed: 22922331]

[16]. Poologasundarampillai G, Wang D, Li S, Nakamura J, Bradley R, Lee PD, Stevens MM, McPhail DS, Kasuga T, Jones JR, Acta Biomater. 2014, 10, 3733. [PubMed: 24874652]

[17]. Jiang J, Carlson MA, Teusink MJ, Wang H, MacEwan MR, Xie J, ACS Biomater. Sci. Eng 2015, 1, 991.

[18]. Boda SK, Thrivikraman G, Panigrahy B, Sarma DD, Basu B, ACS Appl Mater Interfaces 2017, 9, 19389. [PubMed: 27617589]

[19]. Gentleman E, Fredholm YC, Jell G, Lotfibakhshaiesh N, O'Donnell MD, Hill RG, Stevens MM, Biomaterials 2010, 31, 3949. [PubMed: 20170952]

[20]. Xie H, Kang YJ, Curr. Med. Chem 2009, 16, 1304. [PubMed: 19355887]

[21]. Weng L, Boda SK, Teusink MJ, Shuler FD, Li X, Xie J, ACS Appl. Mater. Interfaces 2017, 9, 24484. [PubMed: 28675029]

[22]. Duan G, Jiang S, Jérôme V, Wendorff JH, Fathi A, Uhm J, Altstädt V, Herling M, Breu J, Freitag R, Agarwal S, Greiner A, Adv. Funct. Mater 2015, 25, 2850.

[23]. Tang X, Pikal MJ, Pharm. Res 2004, 21, 191. [PubMed: 15032301]

[24]. Yli-Urpo H, Lassila LVJ, Närhi T, Vallittu PK, Dental Mater. 2005, 21, 201.

[25]. Rahaman MN, Day DE, Sonny Bal B, Fu Q, Jung SB, Bonewald LF, Tomsia AP, Acta Biomater. 2011, 7, 2355. [PubMed: 21421084]

[26]. Bain JL, Bonvallet PP, Abou-Arraj RV, Schupbach P, Reddy MS, Bellis SL, Tissue Eng. Part A 2015, 21, 2426. [PubMed: 26176902]

[27]. Lu T, Li Y, Chen T, Int. J. Nanomedicine 2013, 8, 337. [PubMed: 23345979]

[28]. Dahlin RL, Kasper FK, Mikos AG, Tissue Eng. Part B Rev 2011, 17, 349. [PubMed: 21699434]

[29]. Yao Q, Cosme JG, Xu T, Miszuk JM, Picciani PH, Fong H, Sun H, Biomaterials 2017, 115, 115. [PubMed: 27886552]

[30]. Chen W, Chen S, Morsi Y, El-Hamshary H, El-Newhy M, Fan C, Mo X, ACS Appl. Mater. Interfaces 2016, 8, 24415. [PubMed: 27559926]

[31]. Ziegler C, Wolf A, Liu W, Herrmann A-K, Gaponik N, Eychmüller A, Angew. Chem. Int. Ed 2017, 56, 13200.

[32]. Kim HW, Song JH, Kim HE, J. Biomed. Mater. Res A 2006, 79, 698. [PubMed: 16850456]

[33]. Kim HW, Kim HE, Knowles JC, Adv. Funct. Mater 2006, 16, 1529.

[34]. Pirhonen E, Moimas L, Brink M, Acta Biomater. 2006, 2, 103. [PubMed: 16701864]

[35]. Jariwala SH, Lewis GS, Bushman ZJ, Adair JH, Donahue HJ, 3D Print. Addit. Manuf 2015, 2, 56.

[36]. Garcia-Gonzalez D, Jayamohan J, Sotiropoulos SN, Yoon SH, Cook J, Siviour CR, Arias A, Jérusalem A, J. Mech. Behav. Biomed. Mater 2017, 69, 342. [PubMed: 28160738]

[37]. Duncan RL, Turner CH, Calcif. Tissue Int 1995, 57, 344. [PubMed: 8564797]

[38]. Lee JC, Volpicelli EJ, Adv. Healthcare Mater 2017, 6, 1700232.

[39]. Falcigno L, D'Auria G, Calvanese L, Marasco D, Iacobelli R, Scognamiglio PL, Brun P, Danesin R, Pasqualin M, Castagliuolo I, Dettin M, J. Pept. Sci 2015, 21, 700. [PubMed: 26292841]

[40]. Sun T, Zhou K, Liu M, Guo X, Qu Y, Cui W, Shao Z, Zhang X, Xu S, Tissue Eng J Regen. Med 2017.

[41]. Li J, Hong J, Zheng Q, Guo X, Lan S, Cui F, Pan H, Zou Z, Chen C, J. Orthop. Res 2011, 29, 1745. [PubMed: 21500252]

[42]. Addi C, Murschel F, De Crescenzo G, Tissue Eng. Part B Rev 2017, 23, 163. [PubMed: 27824290]

[43]. Munier P, Gordeyeva K, Bergström L, Fall AB, Biomacromolecules 2016, 17, 1875. [PubMed: 27071304]

[44]. Cho TH, Kim IS, Lee B, Park SN, Ko JH, Hwang SJ, Tissue Eng. Part A 2017.

[45]. Xie J, Blough ER, Wang C-H, Acta Biomater. 2012, 8, 811. [PubMed: 21945829]

[46]. Kokubo T, Biomaterials 1991, 12, 155. [PubMed: 1878450]

[47]. Culpepper BK, Bonvallet PP, Reddy MS, Ponnazhagan S, Bellis SL, Biomaterials 2013, 34, 1506. [PubMed: 23182349]

[48]. Spicer PP, Kretlow JD, Young S, Jansen JA, Kasper FK, Mikos AG, Nat. Protoc 2012, 7, 1918. [PubMed: 23018195]

[49]. O'Reilly MA, Muller A, Hynynen K, Ultrasound Med. Biol 2011, 37, 1930. [PubMed: 21925788]

[50]. Watson BD, Dietrich WD, Busto R, Wachtel MS, Ginsberg MD, Ann. Neurol 1985, 17, 497. [PubMed: 4004172]

[51]. Jiang J, Li Z, Wang H, Wang Y, Carlson MA, Teusink MJ, MacEwan MR, Gu L, Xie J, Adv. Healthcare Mater, 2016, 5, 2993.

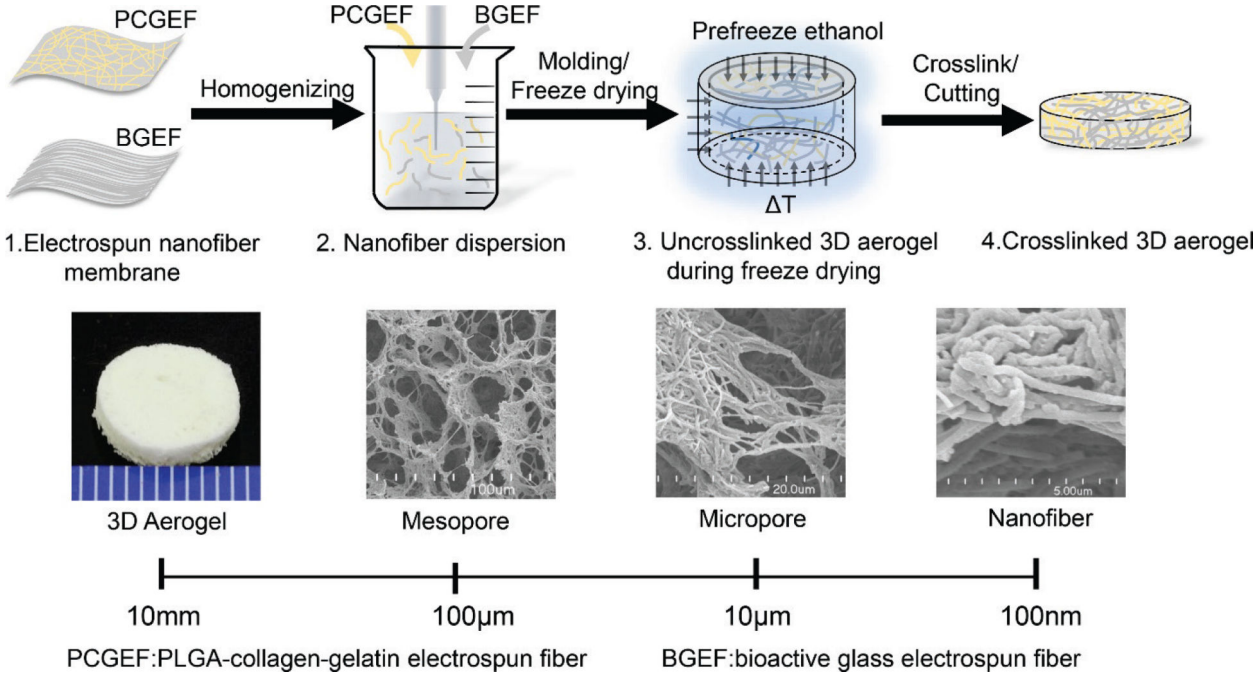

Figure 1.

Schematic illustrating the formation of the 3D hybrid nanofiber aerogel and its structure at different length scales.

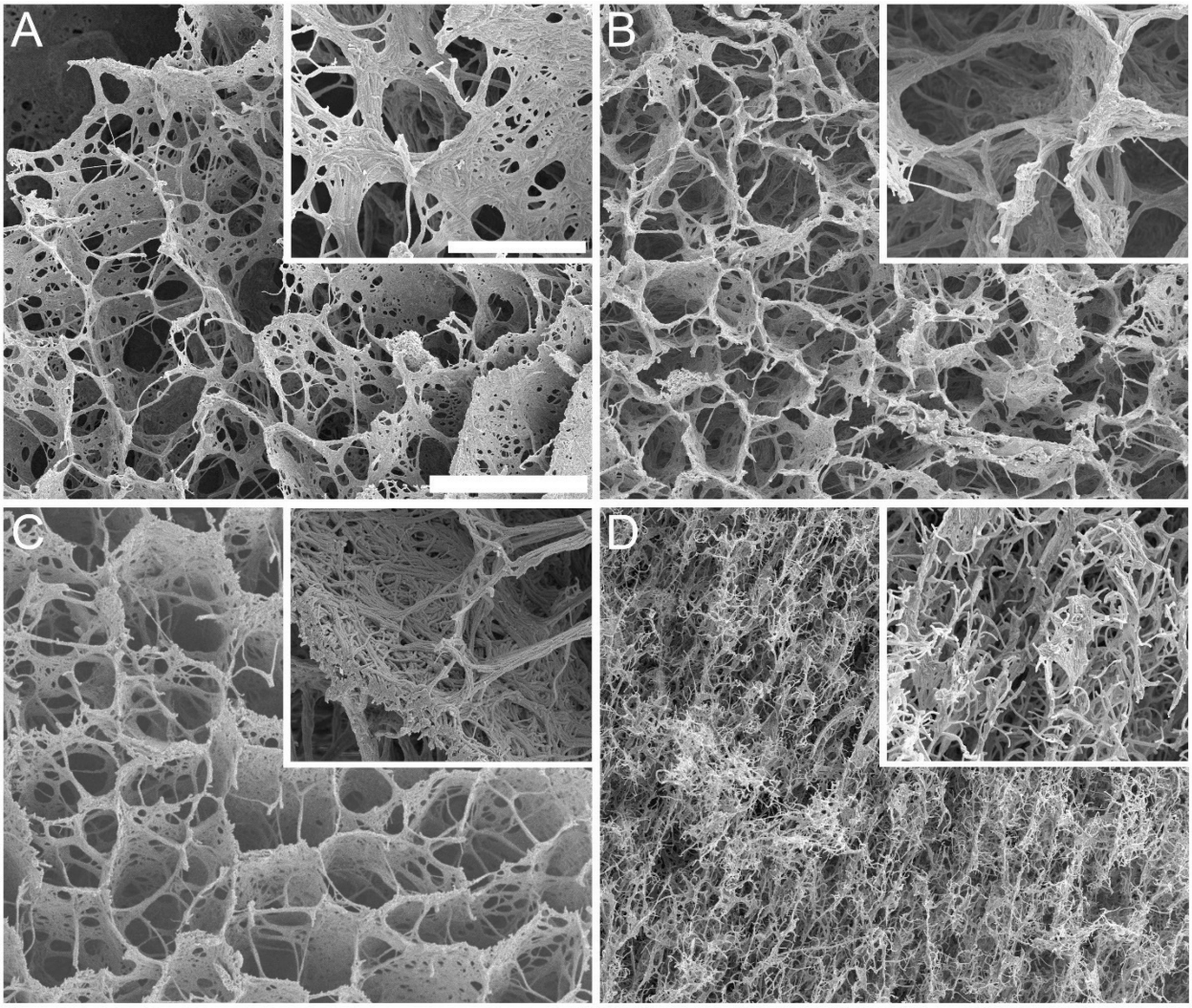

Figure 2.

Effect of freezing temperatures on the structure of 3D hybrid nanofiber aerogels (PCG: BG = 60:40) prior to thermal cross-linking. (A) −30 °C, (B) −50 °C, (C) −80 °C, and (D) −196 °C. Scale bar = 20 μm. Scale bar in the inset = 8 μm.

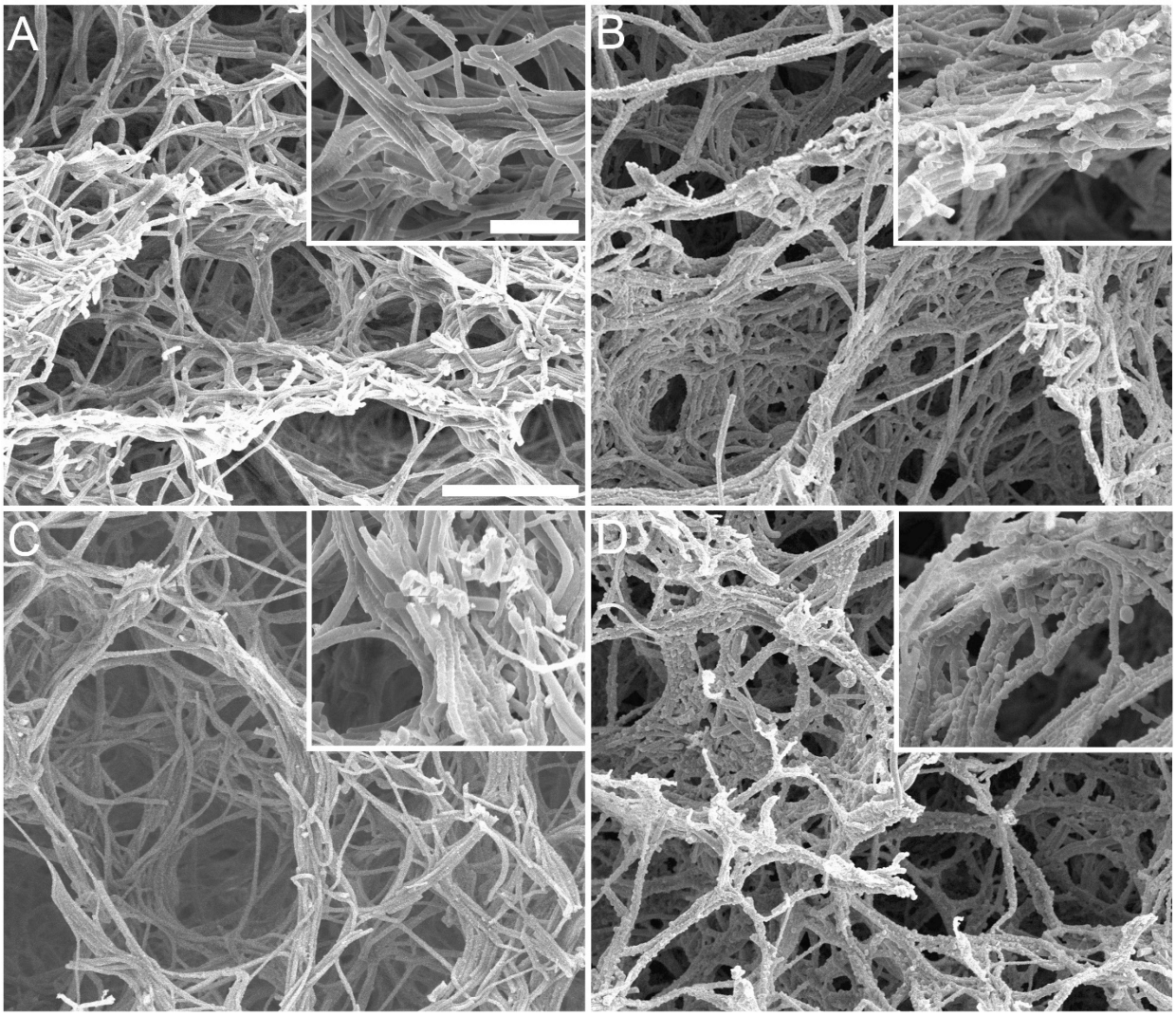

Figure 3.

Effect of thermal cross-linking temperatures and duration on the formation of 3D hybrid nanofiber aerogels (PCG: BG = 60:40, weight ratio). (A) 48 °C for 10 min, (B) 48 °C for 120 min, (C) 52 °C for 10 min, and (D) 52 °C for 120 min. Scale bar = 10 μm. Scale bar in the inset = 2 μm.

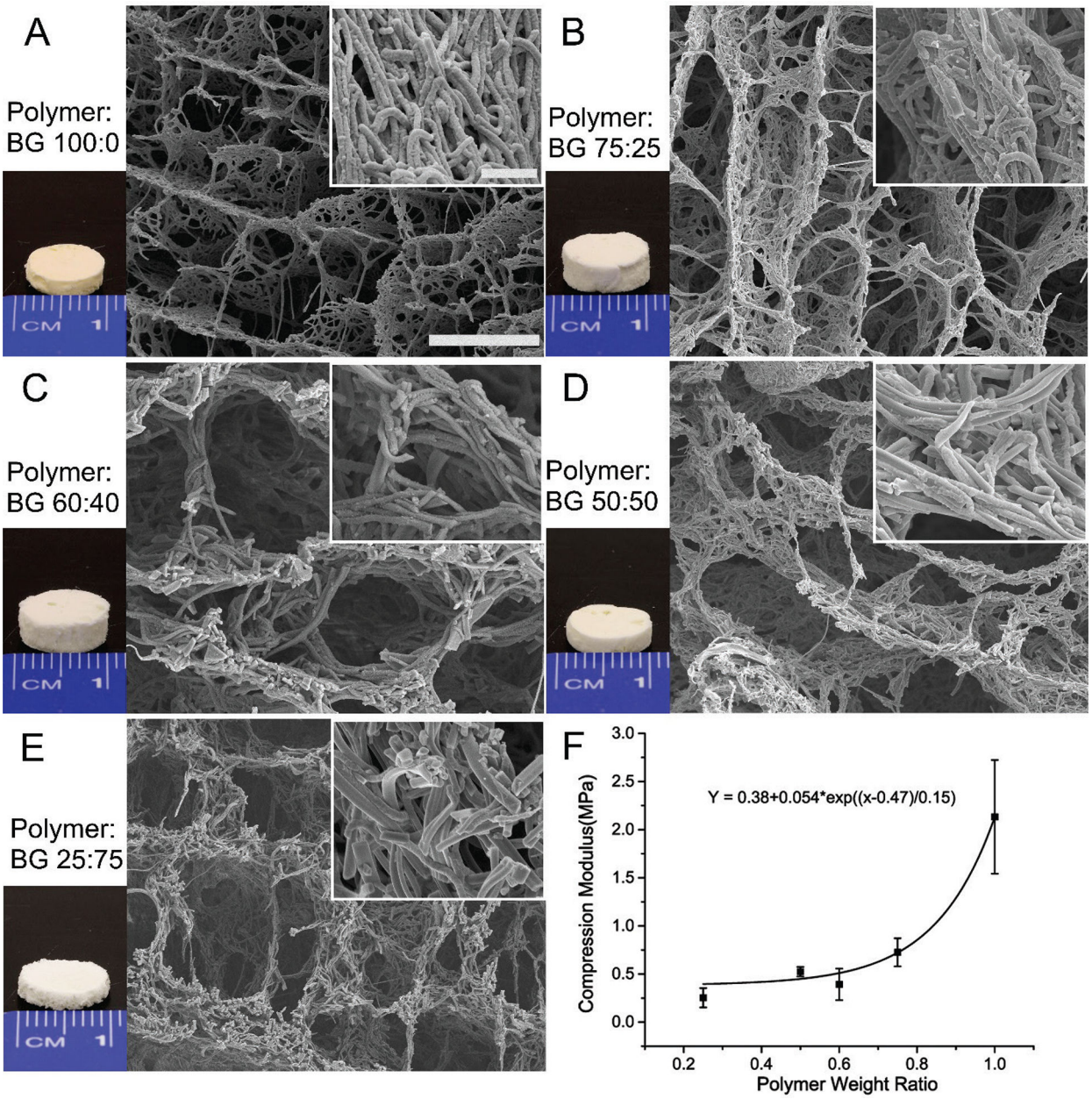

Figure 4.

3D hybrid nanofiber aerogels with different weight ratios of PCG:BG nanofibers and their corresponding mechanic properties. (A) 100:0, (B) 72:25, (C) 60:40, (D) 50:50, (E) 25:75, and (F) the corresponding compressive modulus. Scale bar = 10 μm. Scale in the inset = 2 μm.

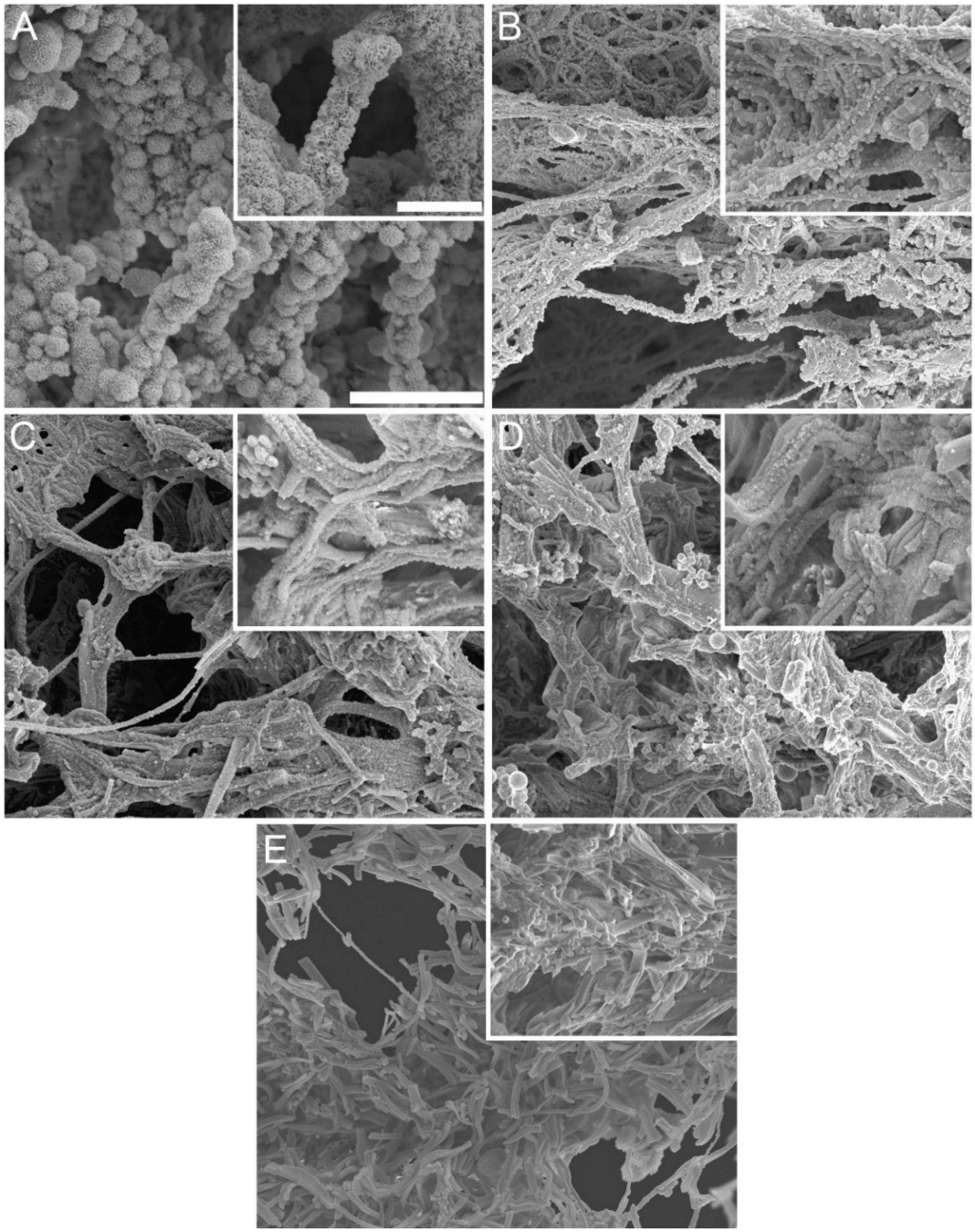

Figure 5.

Biomineralization of 3D hybrid nanofiber aerogels with different ratios of PCG:BG nanofibers in simulated body fluids (SBF) for 2 weeks. (A) 100:0, (B) 75:25 (C) 60:40, (D) 50:50, and (E) 25:75. Scale bar = 10 μm. Scale bar in the inset = 2 μm.

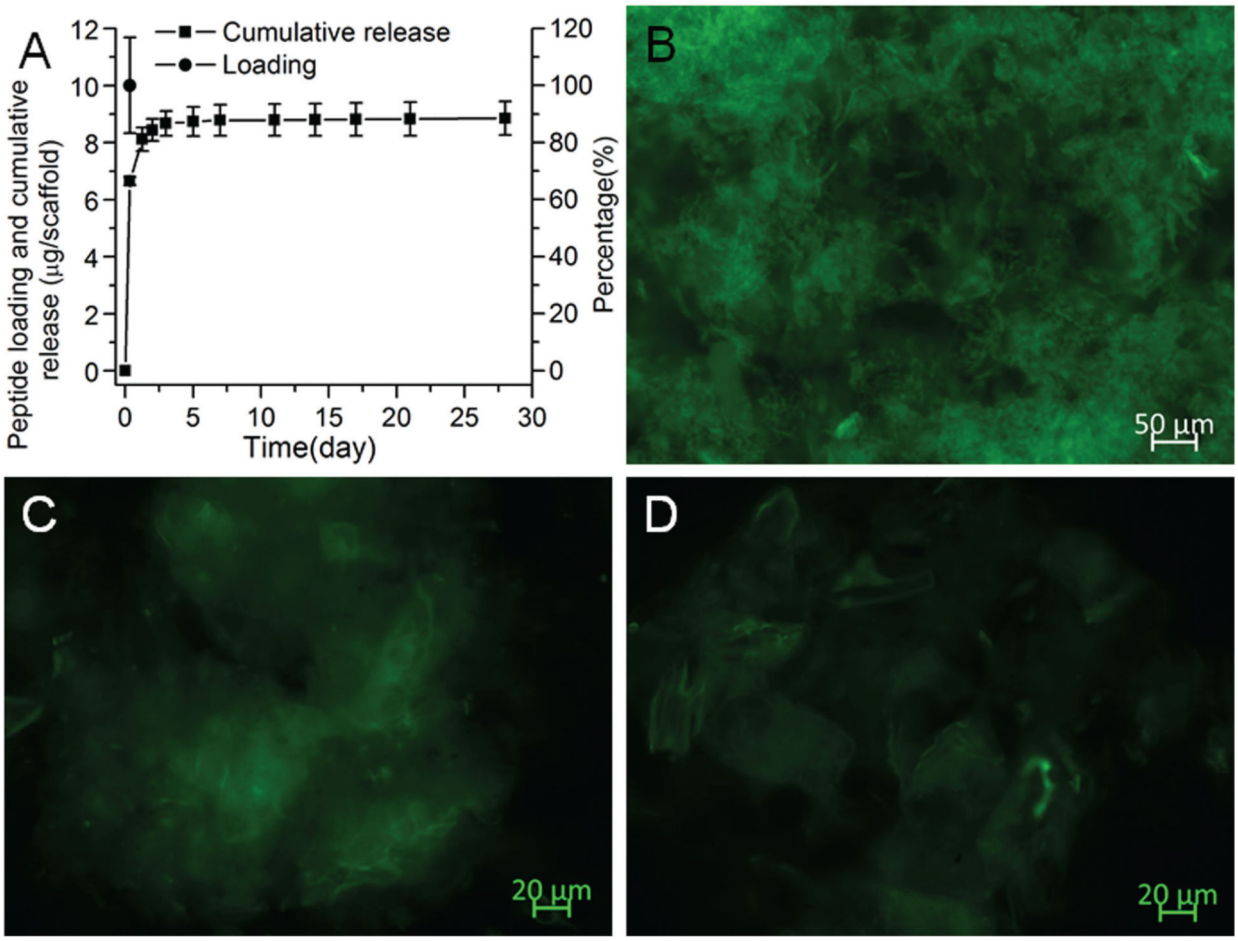

Figure 6.

Adsorption and release of E7-BMP2-FITC peptide on 3D hybrid nanofiber aerogels. (A) Loading of E7-BMP2-FITC peptide on 3D hybrid nanofiber aerogels (PCG:BG = 60:40) by soaking in 35 μg/mL of the peptide solution in TBS for 24 h at room temperature and their cumulative release recorded for 4 weeks. Representative fluorescent images of 3D PCG:BG (60:40) hybrid aerogel (B) after loading, (C) after 21 days of release and (D) 28 days of release.

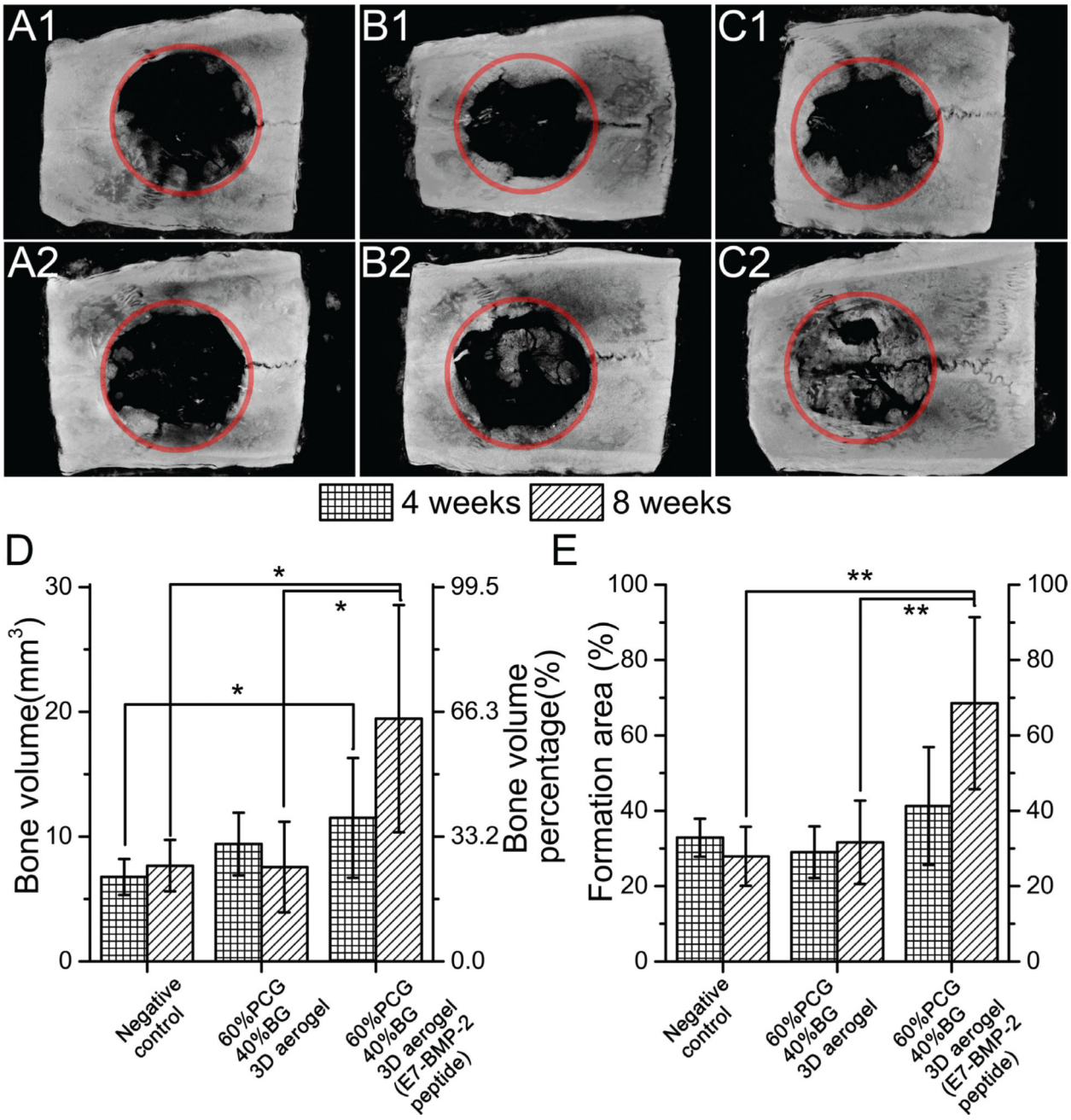

Figure 7.

Representative planar radiographs of cranial bone defects at 4 weeks and 8 weeks after implantation and quantitative analysis. Red circles label the surgery sites. (A1/A2) Without treatment (4w/8w), (B1/B2) 3D hybrid nanofiber aerogel (PCG: BG = 60:40) (4w/8w), (C1/C2) E7-BMP-2 peptide loaded 3D hybrid nanofiber aerogels (PCG: BG = 60:40) (4w/8w), (D) Bone formation areas of various treatments at 4 and 8 weeks, and (E) Regenerated bone volume of various treatments at 4 and 8 weeks. Data shown are mean ± SD of n=12 for each group (n=6 per time point). *$p < 0.05$, **$p < 0.005$.

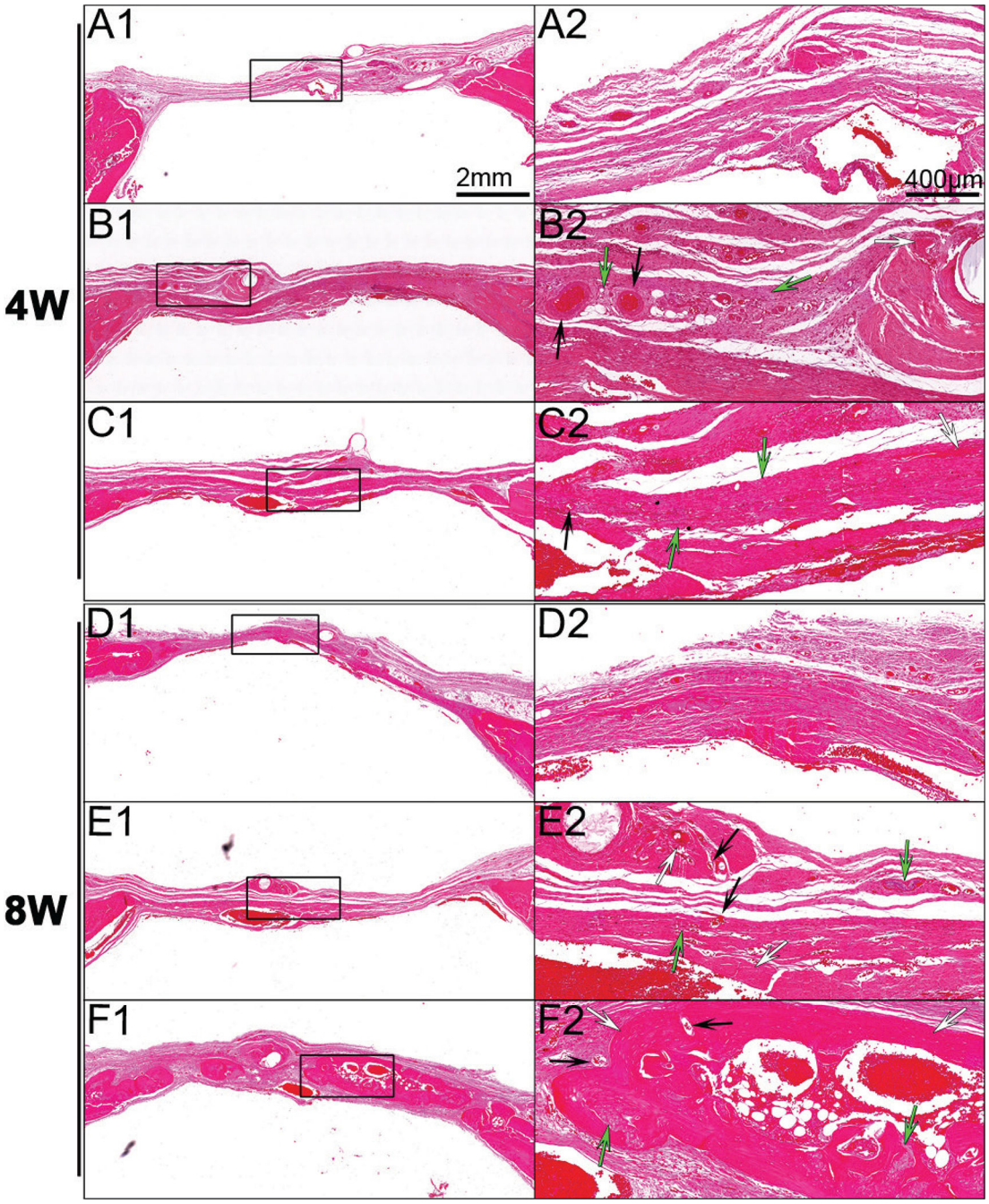

Figure 8.

Hematoxylin and eosin-stained images (4 weeks and 8 weeks after implantation). (A1/A2, D1/D2) Unfilled defect (4w, 8w), (B1/B2, E1/E2) 3D hybrid nanofiber aerogel (PCG:BG = 60:40) (4w, 8w), (C1/C2, F1/F2) E7-BMP-2 peptide loaded 3D hybrid nanofiber aerogel (PCG:BG = 60:40) (4w, 8w). (Black arrow: blood vessel in aerogel; white arrow: aerogel residue; green arrow: new bone.)

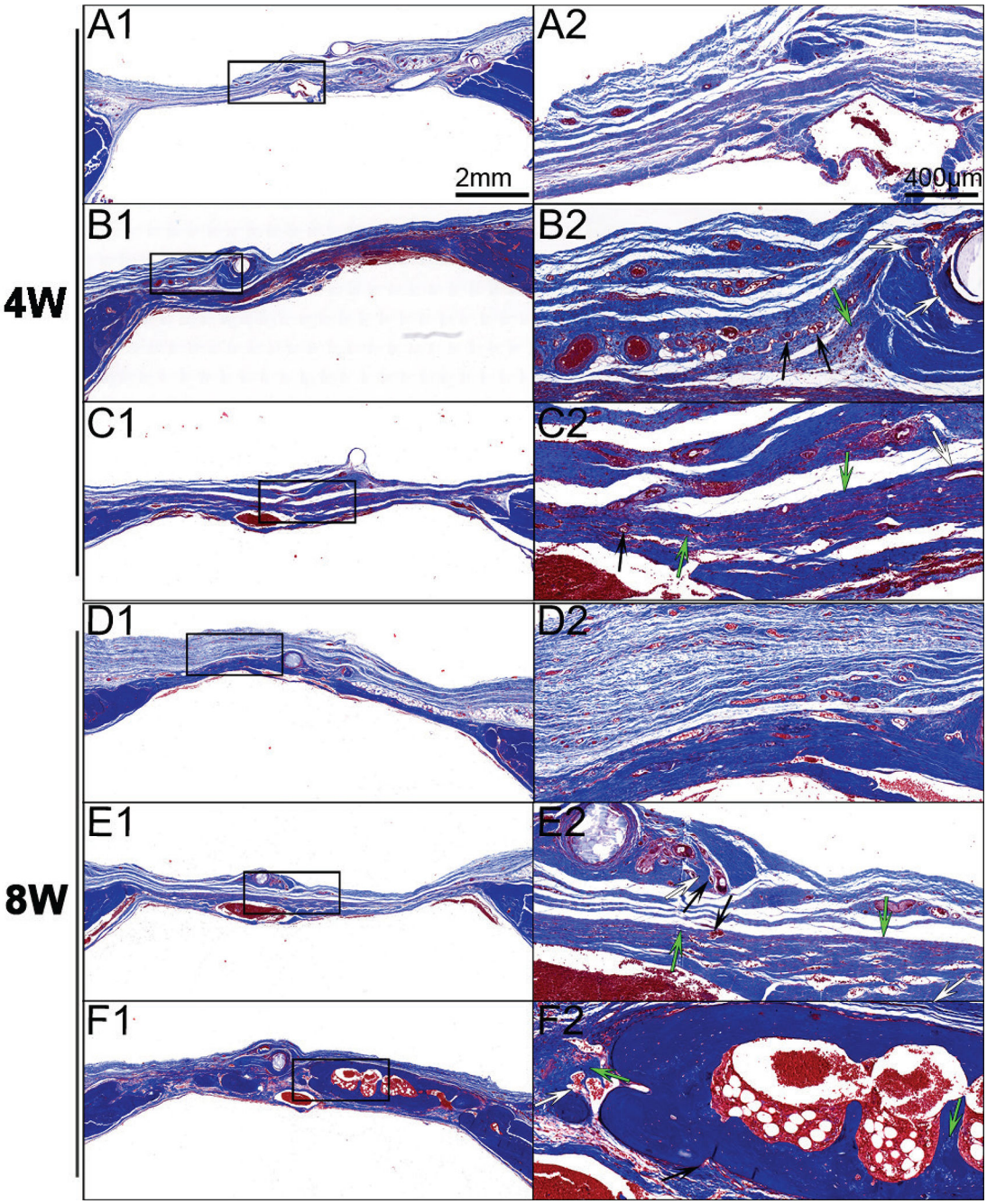

Figure 9.

Masson's Trichrome stained images. (4 weeks and 8 weeks after implantation). (A1/A2, D1/D2) Unfilled defect (4w, 8w), (B1/B2, E1/E2) 3D hybrid nanofiber aerogel (PCG:BG = 60:40) (4w, 8w), (C1/C2, F1/F2) E7-BMP-2 peptide loaded 3D hybrid nanofiber aerogel (PCG:BG = 60:40) (4w, 8w). (Black arrow: blood vessel in aerogel; white arrow: aerogel residue; green arrow: new bone.)

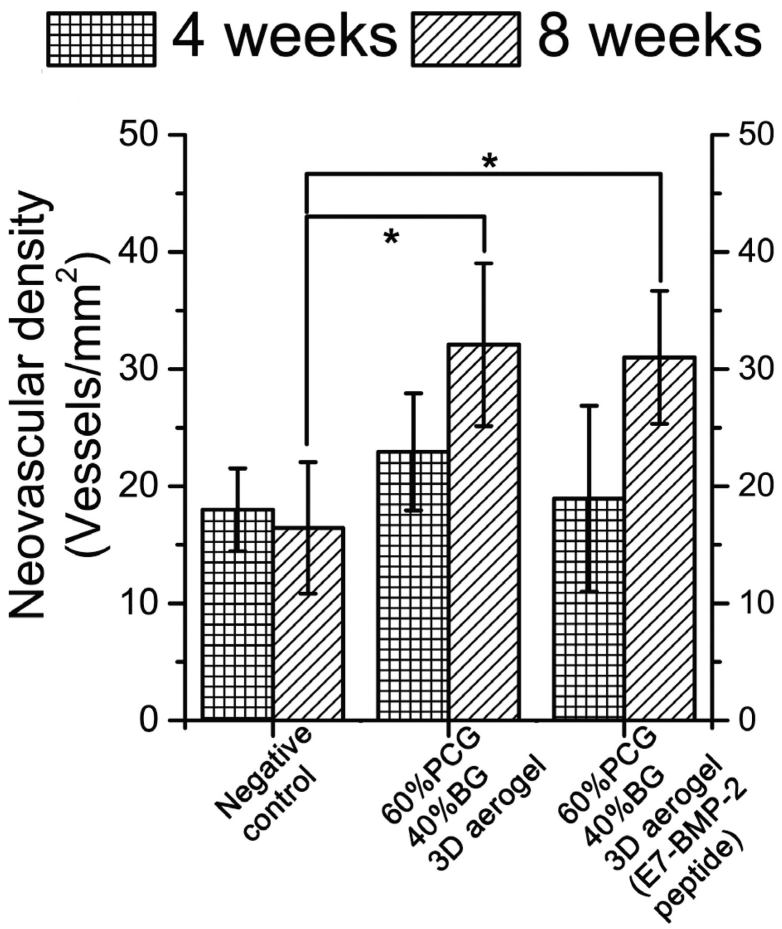

Figure 10.

Neovascularization of the regenerated tissue in the calvarial bone defect for different implantation groups after 4 and 8 weeks of surgery. Data presented are mean ± SD of analysis of 12 slides/ histological sections per group. * $p < 0.05$ (n=12)